Four-wave mixing in a quantum cascade laser amplifier

Peter Friedli,[1,a)] Hans Sigg,[1,a)] Borislav Hinkov,[2] Andreas Hugi,[2] Sabine Riedi,[2] Mattias Beck,[2] and Jérôme Faist[2,a)]
[1]*Laboratory for Micro- and Nanotechnology, Paul Scherrer Institute, CH-5232 Villigen, Switzerland*
[2]*Institute for Quantum Electronics, ETH Zurich, CH-8093 Zurich, Switzerland*

(Received 29 March 2013; accepted 6 May 2013; published online 4 June 2013)

We present the direct observation of four-wave mixing over a detuning range of more than 3 THz in an InGaAs/AlInAs strain-compensated quantum cascade laser (QCL) amplifier emitting at 4.3 μm by simultaneous injection of a single mode QCL and a broadly tunable source. From its intensity, we determine a $\chi^{(3)}$ of 0.9×10^{-15} m^2 V^{-2}, in good agreement with transport model simulations based on the density matrix approach. This four-wave-mixing mechanism is an important driving factor in mode proliferation occurring in connection with the recent demonstration of comb generation in broadband QCLs. © *2013 AIP Publishing LLC*.
[http://dx.doi.org/10.1063/1.4807662]

Intersubband transitions in quantum wells are attractive building blocks for devices such as quantum well detectors,[1] lasers,[2] and artificial nonlinear materials[3] because of the large value of their dipole matrix element, combined with the tailorability of the system. Recently, a quantum cascade laser (QCL) frequency comb was demonstrated,[4] offering the potential for broadband multiheterodyne spectroscopy[5] in the mid-infrared spectral region. Similar as in microresonators,[6] the mode proliferation needed for the comb generation was ascribed to a four-wave-mixing (FWM) process occurring between adjacent longitudinal cavity modes. This FWM mechanism is an important driving factor in mode proliferation in broadband QCLs as well as opening up further opportunities for ultra-fast wavelength conversion applications.

Large values of the nonlinear coefficient, surpassing the bulk value by many orders of magnitude,[7] were measured in intersubband systems. In particular, resonant third-order nonlinearity was responsible for enhanced third harmonic generation[8] and FWM experiments[9] in doped quantum well systems. In a QCL, an equally large value of $\chi^{(3)}$ is expected to arise from both virtual transitions and real population inversion modulation. The latter effect, corresponding to a time-dependent spatial hole burning, is very efficient in QCLs because, in contrast to interband semiconductor lasers, transport as well as intersubband scattering is much faster than the in-plane carrier diffusion time.[10]

Early FWM experiments performed in interband lasers also ascribed the nonlinearity to the presence of a moving gain grating created by spatial hole burning[11] and, therefore, the FWM signal was strongly attenuated when the detuning between pump and signal waves increased beyond a few Gigahertz. In contrast, the bandwidth of the FWM in QCLs is expected to be much wider because of the much shorter timescales involved.

The investigated mid-infrared QCL amplifier was grown in the strain-balanced $In_{0.725}Ga_{0.275}As/In_{0.276}Al_{0.724}As$ system by molecular beam epitaxy with a sheet carrier density of 1.5×10^{11} cm^{-2} on an n-doped InP wafer. It emits at 4.3 μm. A standard buried-heterostructure process was used to define waveguides with widths of approximately 7 μm. The details of the active region are published elsewhere.[12] Prior to measurement, both facets of the device were provided with an anti-reflection (AR) coating with a single layer of Al_2O_3. As shown schematically in Fig. 1(a), the pump source operating at ω_1 is a tunable laser source with 100 ps pulse length, based on optical parametric amplification with difference frequency generation (DFG), as described in Ref. 13, while the probe laser at $\omega_2 = \omega_1 + \delta\omega$ is a narrow-linewidth distributed feedback (DFB) QCL.[14] The DFB QCL contains a first-order grating in the top waveguide confinement layer to allow for single-mode emission. Both sources are coupled into the QCL amplifier using Ge lenses with a high numerical aperture. The output light of the QCL

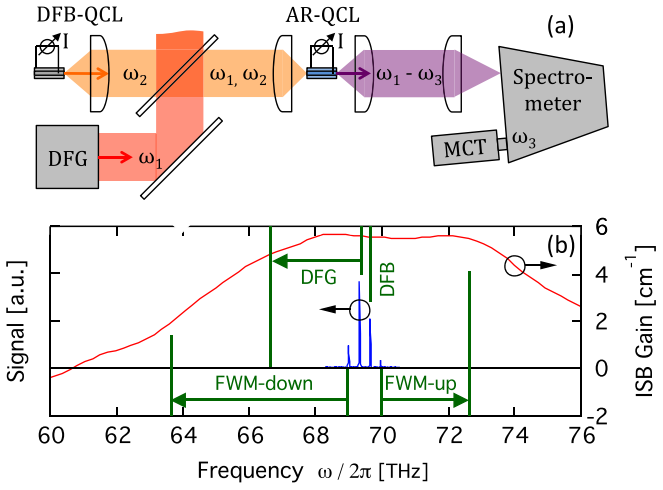

FIG. 1. (a) Experimental setup, which couples the 100 ps long DFG pump pulse and ~30 ns long DFB-QCL probe pulse to the AR-QCL. A grating spectrometer is used to disperse the output signal, which is measured by an 800 MHz bandwidth MCT detector. (b) A typically measured output spectrum is shown in blue color. The green lines mark the maximum performed frequency tuning range. The ISB gain of the AR-QCL at the used current density measured using synchrotron IR micro-spectroscopy is given in red color.

[a)]Electronic addresses: pfriedli@gmail.com, hans.sigg@psi.ch, and jerome.faist@phys.ethz.ch

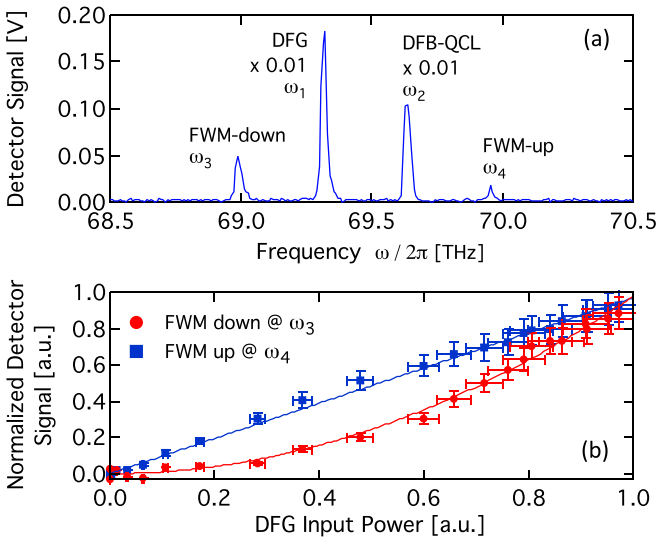

FIG. 2. (a) The measured spectrum of the FWM for a frequency difference $\delta\omega = 2\pi \times 314$ GHz showing the FWM peaks at the locations expected by energy conservation, i.e., $\omega_3 = 2\omega_1 - \omega_2$ and $\omega_4 = 2\omega_2 - \omega_1$. An additional 1% transmission optical filter was used during the measurement at the DFG and DFB-QCL frequencies to protect the sensitive detector. (b) The normalized FWM signals with respect to the continuously increased input power of the DFG match to the linear and quadratic behavior, as expected for FWM.

amplifier is then dispersed by a grating spectrometer, and subsequently detected by fast 800 MHz bandwidth mercury cadmium telluride (MCT) detector. The amplified IR transmission of the QCL, used for the gain estimate, is measured by synchrotron IR micro-spectroscopy.[15] The result is given in Fig. 1(b), along with the frequency-tuning range of the pump, probe, and detected signals. Both QCL devices are run at room temperature in pulsed conditions at a low duty cycle excitation <1%.

A typical spectrum consisting of the pump, probe, and FWM contributions is shown in Fig. 2 for a splitting $\delta\omega = 2\pi \times 314$ GHz. In addition to the signals at ω_1, ω_2, and the expected FWM signal at $\omega_3 = 2\omega_1 - \omega_2 = \omega_1 - \delta\omega$, a fourth, weaker peak is observed at $\omega_4 = 2\omega_2 - \omega_1 = \omega_2 + \delta\omega$, which corresponds to the mixing of two probe photons with one photon from the (here stronger) pump. During the measurement at the pump and probe frequencies, the detector was protected by an additional 1% transmission neutral density filter. For the determination of the peak power below, the measured detector amplitude of the DFG- and the FWM-pulses is corrected for the bandwidth-limited detection by a factor of 7.5 (determined from the convolution of the 100 ps pulse with an 800 MHz low-pass) and calibrated against the power measured using a thermal detector. Coupling and collection efficiencies are taken into account by measuring the relative transmission of the relevant lenses and the grating spectrometer.

In Fig. 2(b), the power of the resulting FWM-signals is shown with respect to the DFG pump power. The FWM output power is quadratic and linear in the pump (DFG) P_1 and probe (DFB-QCL) P_2 powers, respectively, i.e., $P_3 \propto \chi^{(3)} P_1^2 P_2$ (for the lower FWM frequency) and $P_4 \propto \chi^{(3)} P_1 P_2^2$ (for the upper FWM frequency), where $\chi^{(3)}$ is the third-order nonlinear optical susceptibility and P_i is the peak power for each mode. Because of $P_1,\ P_2 \gg P_3,\ P_4$, we can neglect the effect of the FWM signal ω_4 on ω_3, and model the behavior with degenerate FWM.

In the following, the electrical fields E_k are described by the slowly varying envelope approximation $E_k = A_k \exp(-i\beta_k z)$. For the determination of $\chi^{(3)}$, we use the coupled waves theory[16,17] to describe the evolution of the involved optical waves in the waveguide undergoing a perturbation of the polarization. The system of differential equations is solved for the amplitude A_3 of the FWM-down signal

$$A_3 = \frac{\kappa}{g - i\Delta\beta}\left[\exp\left[\left(\frac{3}{2}g - i\Delta\beta\right)z\right] - \exp\left(\frac{g}{2}z\right)\right], \qquad (1)$$

where

$$\kappa = \frac{-i\mu_0\epsilon_0\omega_3^2\chi^{(3)}}{8\beta_3} 3A_1^2 A_2$$

describes the nonlinear mixing from the two input fields, g is the measured wavelength-dependent gain, μ_0 and ε_0 are the permeability and permittivity, respectively, $\chi^{(3)}$ is the third-order susceptibility, β_3 is the propagation constant, and $A_{1,2}$ are the amplitudes of pump and probe fields. The phase-matching condition $|\Delta\beta| = |2\beta_1 - \beta_2 - \beta_3| = 0$ is considered to be satisfied, if $\Delta\beta \times L \ll 2\pi$, i.e., $|\frac{\partial n_g}{\partial\lambda}|\ \frac{\delta\omega^2}{\omega_1^2}\ L \ll 1$, as given in Ref. 18. For the very low group velocity dispersion below 0.01 μm^{-1} observed in QCLs[4,19] and the used cavity length L = 3 mm, this results in $\delta\omega \ll 2\pi \times 12$ THz, which is well below the applied frequency detuning $\delta\omega$ in this work. Hence, the group velocity dispersion $\Delta\beta$ in Eq. (1) can be neglected. We then use the boundary conditions $A_3(z=0) = 0$ and the measured output fields for the minimum $\delta\omega_{min} = 210$ GHz at $z = L$, i.e., $E_1 = 644$ kV/m, $E_2 = 544$ kV/m, and $E_3 = 5$ kV/m, as obtained by $E_i = \sqrt{\frac{2I_i}{c\,\varepsilon_0\,n}}$, where $I_i = P_i/A$ is the intensity of each field with waveguide cross-section area A = 16 μm^2 and the measured peak powers are $P_1 = 30$ mW, $P_2 = 21.4$ mW, and $P_3 = 0.16$ mW, respectively. The peak gain g within the AR-QCL is measured to be 5.7 cm^{-1} close to the roll-over of the device. We finally obtain $\chi^{(3)} = (0.9 \pm 0.2) \times 10^{-15}\ m^2\,V^{-2}$ for these experimental conditions.

For comparison, we model $\chi^{(3)}$ by assuming a two-level system[20] with a dephasing characterized by the dephasing time $T_2 = 0.15$ ps and the relaxation time $T_1 = 0.29$ ps. The time values are determined from transport model simulations based on the density matrix approach.[21] Assuming the low field limit (i.e., the condition $\Omega_R T_2 \ll 1$, where $\Omega_R = \frac{q\,z_{ij}\,E}{\hbar}$), we obtain for the nonlinear coefficient

$$\chi^{(3)}(\Delta, \delta\omega) = \frac{2\delta N_0 (q \cdot z_{ij})^4}{3\epsilon_0\hbar^3} \frac{(\delta\omega - \Delta - i/T_2)(-\delta\omega + 2i/T_2)(\Delta + i/T_2)^{-1}}{(\Delta - \delta\omega + i/T_2)(\delta\omega - i/T_1)(\delta\omega - \Delta - i/T_2)(\delta\omega + \Delta - i/T_2)}, \qquad (2)$$

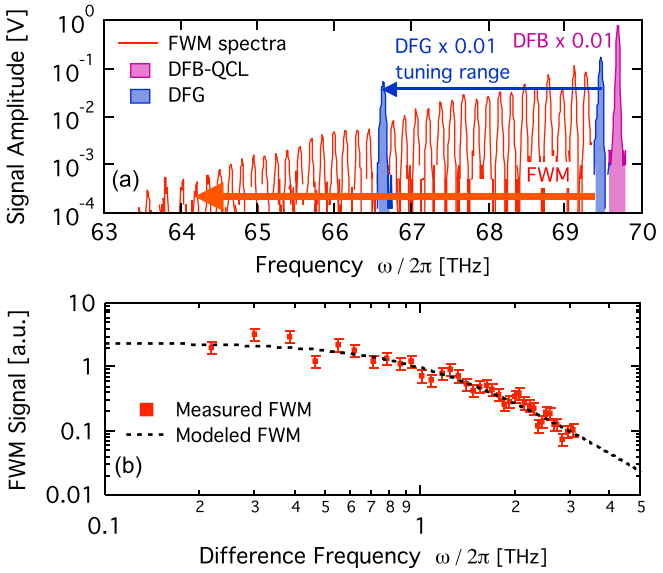

FIG. 3. (a) Measured output spectra of the FWM (red) for the frequency tuning of the DFG between 69.5 and 66.7 THz (blue curves), and the fixed-frequency DFB-QCL (magenta). (b) Integrated and normalized intensity of the FWM signal versus the difference frequency $\delta\omega$ between DFB-QCL and DFG up to a maximum detuning of 3.06 THz. The integral is normalized with respect to DFG input power and spectral gain of the AR-QCL, and matches well to the modeled third-order nonlinearity.

where δN_0 is the volume population inversion per QC period (47.5 nm), q is the electric charge, $z_{ij} = 1.6$ nm is the dipole moment computed for this structure, $\hbar$ is the reduced Plank's constant, and $\Delta = \omega_1 - \omega_{12}$ is the detuning from the inter-subband transition at 290 meV. The value obtained is $\chi^{(3)} = 2.5 \times 10^{-15}\,\mathrm{m^2\,V^{-2}}$, and matches well our measurement given the uncertainties in the experimental and modeled parameters and taking into account the overlap factor of the optical mode with the active region.

In Fig. 3(a), we give the spectra for the fixed-frequency DFB-QCL, the range of DFG tuning, together with a series of FWM-down spectra. The mixing efficiency from the input fields to the FWM signals was observed to be approximately −20 dB in peak power. The integrals of the FWM spectra, taking into account the spectral gain dependence given in Fig. 1 and normalized to the DFG input power, directly result in the efficiency of the FWM process, which is proportional to $\chi^{(3)}$. The normalized data are shown in Fig. 3(b). The measured roll-off of the response as a function of the difference frequency matches well the frequency behavior of Eq. (2) and hence confirms the model.

As shown in Fig. 4, for the case of an uncoated Fabry-Pérot QCL (FP-QCL) with facet reflectivities of ∼27%, strong mode competition arises. As a result, when the FP-QCL is driven close to laser threshold, the amplification of the pump, probe, and the FWM signals exhibits nonlinearities as a function of the input power of the DFG pump. Interestingly, the FWM-down signal here only emerges above a certain DFG input power, while the FWM-up signal, which depends quadratically on the constant strong DFB field, arises immediately. For a proper modeling of these effects, both cavity feedback and the loss modulation due to spatial hole burning would need to be taken into account, which all add up to intensity variations in multimode operation, as observed in Ref. 10.

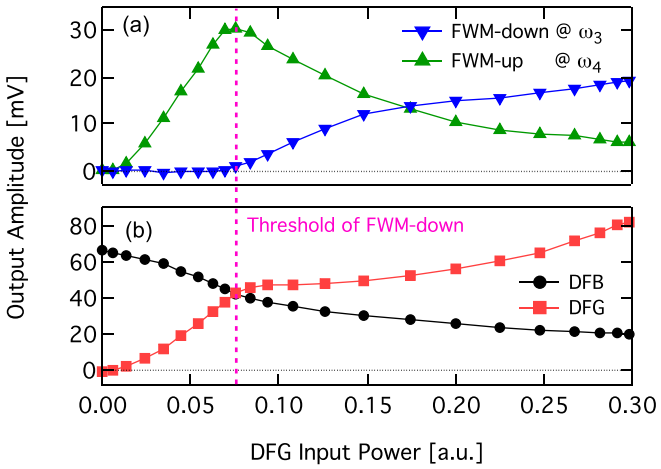

FIG. 4. (a) Measured injection-intensity dependence of the output power at the respective wavelengths for increasing DFG input power for constant DFB-QCL and FP-QCL pumping. The detected FWM-down signal reveals a threshold behavior, contrary to the FWM-up signal. (b) Amplified DFG and DFB output power. The decrease in DFB amplification is due to the gain drain with increased DFG input power.

In summary, the maximum observed frequency detuning frequency of $\delta\omega_{max} = 2\pi \times 3.05$ THz is more than two orders of magnitude higher than the FP mode spacing $\delta\omega_{FP} = 2\pi \times 15$ GHz in a typical laser cavity with a length of 3 mm. Together with the observed conversion efficiency that is above −40 dB over nearly the full measured detuning range, and thus sufficient for passive FM mode-locking,[22] we present a relevant FWM mechanism for driving the mode proliferation for comb generation in broadband QCLs.[4] The unambiguously achieved assignment to the intrinsic nonlinear property of the QCL structure opens up further opportunities for flexible and ultra-fast wavelength conversion, which so far is established only in the telecommunications wavelength range around 1.5 μm. Together with the recent demonstration of room temperature operation in continuous wave with very low dissipation,[14] QCLs could hence serve for autonomous spectroscopy and communications applications in the mid-infrared spectral region by using compact, all solid-state devices.

The Swiss National Science Foundation (SNSF) funded part of this work. We would like to thank Dr. Philippe Lerch and Stefan Stutz for technical support. Gain measurement was performed at the IR beamline X01DC of the Swiss Light Source SLS.

[1]H. Schneider and H. C. Liu, *Quantum Well Infrared Photodetectors* (Springer, Berlin, 2007).
[2]J. Faist, F. Capasso, D. L. Sivco, C. Sirtori, A. Hutchinson, and A. Y. Cho, Science **264**, 553 (1994).
[3]E. Rosencher, A. Fiore, B. Vinter, V. Berger, P. Bois, and J. Nagle, Science **271**, 168 (1996).
[4]A. Hugi, G. Villares, S. Blaser, H. C. Liu, and J. Faist, Nature **492**, 229 (2012).
[5]F. Keilmann, C. Gohle, and R. Holzwarth, Opt. Lett. **29**, 1542 (2004).
[6]T. J. Kippenberg, R. Holzwarth, and S. A. Diddams, Science **332**, 555 (2011).
[7]C. Sirtori, F. Capasso, D. L. Sivco, S. N. G. Chu, and A. Y. Cho, Appl. Phys. Lett. **59**, 2302 (1991).
[8]C. Sirtori, F. Capasso, D. Sivco, and A. Cho, Phys. Rev. Lett. **68**, 1010 (1992).

[9]D. Walrod, S. Y. Auyang, P. A. Wolff, and M. Sugimoto, Appl. Phys. Lett. **59**, 2932 (1991).
[10]A. Gordon, C. Y. Wang, L. Diehl, F. X. Kartner, A. Belyanin, D. Bour, S. Corzine, G. Hofler, H. C. Liu, and H. Schneider, Phys. Rev. A **77**, 053804 (2008).
[11]K. Inoue, T. Mukai, and T. Saitoh, Appl. Phys. Lett. **51**, 1051 (1987).
[12]A. Bismuto, R. Terazzi, B. Hinkov, M. Beck, and J. Faist, Appl. Phys. Lett. **101**, 021103 (2012).
[13]L. Carroll, P. Friedli, P. Lerch, J. Schneider, D. Treyer, S. Hunziker, S. Stutz, and H. Sigg, Rev. Sci. Instrum. **82**, 063101 (2011).
[14]B. Hinkov, A. Bismuto, Y. Bonetti, M. Beck, S. Blaser, and J. Faist, Electron. Lett. **48**, 646 (2012).
[15]P. Friedli, H. Sigg, A. Wittmann, R. Terazzi, M. Beck, A. Kolek, and J. Faist, Appl. Phys. Lett. **102**, 012112 (2013).
[16]G. P. Agrawal, Appl. Phys. Lett. **51**, 302 (1987).
[17]M. Yamada, J. Appl. Phys. **66**, 81 (1989).
[18]A. Uskov, J. Mork, and J. Mark, IEEE J. Quantum Electron. **30**, 1769 (1994).
[19]C. Gmachl, A. Soibel, R. Colombelli, D. L. Sivco, F. Capasso, and A. Y. Cho, IEEE Photonics Technol. Lett. **14**, 1671 (2002).
[20]R. Boyd, *Nonlinear Optics* (Academic Press, 2008).
[21]R. Terazzi and J. Faist, New J. Phys. **12**, 033045 (2010).
[22]L. F. Tiemeijer, P. I. Kuindersma, P. J. A. Thijs, and G. L. J. Rikken, IEEE J. Quantum Electron. **25**, 1385 (1989).